The Influence of Soil Moisture, Coastline Curvature, and Land-Breeze Circulations on Sea-Breeze-Initiated Precipitation

R. DAVID BAKER

Mesoscale Atmospheric Processes Branch, NASA Goddard Space Flight Center, Universities Space Research Association, Greenbelt, and Joint Center for Earth Systems Technology, University of Maryland, Baltimore County, Baltimore, Maryland

BARRY H. LYNN

Mesoscale Atmospheric Processes Branch, NASA Goddard Space Flight Center, Greenbelt, Maryland, and Center for Climate Systems Research, Columbia University, New York City, New York

AARON BOONE

Centre National de Recherches Météorologiques, Météo-France, Toulouse, France

WEI-KUO TAO

Mesoscale Atmospheric Processes Branch, NASA Goddard Space Flight Center, Greenbelt, Maryland

JOANNE SIMPSON

Laboratory for Atmospheres, NASA Goddard Space Flight Center, Greenbelt, Maryland

(Manuscript received 7 March 2000, in final form 22 November 2000)

ABSTRACT

Idealized numerical simulations of Florida convection are performed with a coupled atmosphere–land surface model to identify the roles of initial soil moisture, coastline curvature, and land-breeze circulations on sea-breeze-initiated precipitation. The 3D Goddard Cumulus Ensemble cloud-resolving model is coupled with the Goddard Parameterization for Land–Atmosphere–Cloud Exchange land surface model, thus providing a tool to simulate more realistically land surface–atmosphere interaction and convective initiation. Eight simulations are conducted with either straight or curved coastlines, initially homogeneous soil moisture or initially variable soil moisture, and initially homogeneous horizontal winds or initially variable horizontal winds (land breezes). An additional simulation is performed to assess the role of Lake Okeechobee on convective development.

All model simulations capture the diurnal evolution and general distribution of sea-breeze-initiated precipitation over central Florida. The distribution of initial soil moisture influences the timing and location of subsequent precipitation. Soil moisture acts as a moisture source for the atmosphere, increases the convectively available potential energy, and thus preferentially focuses heavy precipitation over existing wet soil. Soil moisture–induced mesoscale circulations do not produce heavy precipitation. Coastline curvature has a major impact on the timing and location of precipitation. Earlier low-level convergence occurs inland of convex coastlines, and subsequent heavy precipitation occurs earlier in simulations with curved coastlines. Early-morning land breezes influence the timing of precipitation by modifying low-level convergence. Because of nonlinear interaction between coastline curvature and soil moisture, the highest peak accumulated rainfall and highest peak rain rates occur in simulations with both coastline curvature and initial soil moisture variations. Lake Okeechobee influences the timing and location of precipitation because of strong lake-breeze circulations.

1. Introduction

It has long been recognized that sea breezes strongly influence development of deep cumulus convection over the Florida peninsula (e.g., Byers and Rodebush 1948; Pielke 1974; Simpson et al. 1980; Blanchard and Lopez 1985; Fankhauser et al. 1995; Kingsmill 1995; Wilson and Megenhardt 1997). Under synoptically undisturbed conditions, convection can develop along boundary layer convergence lines associated with sea breezes from the east and west coasts of Florida. Depending on the mean wind direction, cold outflow from convection along a sea-breeze front may interact with the sea-breeze convergence zone from the other coast and produce strong thunderstorms (Fankhauser et al. 1995; Kingsmill 1995; Wilson and Megenhardt 1997). The location and

Current affiliation: Department of Physics, Austin College, Sherman, Texas.

Corresponding author address: Dr. R. David Baker, Physics Department, Austin College, 900 North Grand Ave., Sherman, TX 75090. E-mail: dbaker@austinc.edu

intensity of precipitation associated with Florida sea breeze circulations is thus directly influenced by factors that control low-level convergence. In this paper, we explore the role of three factors on sea-breeze-initiated precipitation over the Florida peninsula: soil moisture availability, coastline curvature, and early morning land-breeze circulations.

Soil moisture may affect convective development by enhancing atmospheric moisture or by modulating the surface temperature to produce mesoscale circulations. Through strong evapotranspiration, wet soil may act as a moisture source for the overlying atmospheric boundary layer, thus increasing the moist static energy of the atmosphere and promoting convective development (e.g., Segal et al. 1995; Clark and Arritt 1995; Taylor et al. 1997; Eltahir 1998). In numerical simulations with weak winds, horizontal variations in soil moisture have been shown to produce strong mesoscale circulations (e.g., Ookouchi et al. 1984; Yan and Anthes 1988; Avissar and Liu 1996; Lynn et al. 1998). Clouds and subsequent rainfall may develop along the soil moisture–induced frontal boundary (Avissar and Liu 1996; Lynn et al. 1998). However, there is little direct observational evidence for soil moisture–induced circulations, except perhaps in irrigated fields under light winds (Segal and Arritt 1992; Doran et al. 1992).

The role of soil moisture on Florida precipitation remains unclear. Two-dimensional simulations indicate that moist surface conditions and dry surface conditions produce comparable rainfall amounts over the Florida peninsula (Nicholls et al. 1991), but three-dimensional simulations suggest peak precipitation amounts 6 times larger for dry soil than for moist soil (Xu et al. 1996). In both 2D and 3D simulations, soil moisture significantly altered the distribution of precipitation (Nicholls et al. 1991; Xu et al. 1996).

Coastline curvature also may modulate sea-breeze convergence. Idealized numerical simulations indicate that convex coastlines exhibit strong convergence and concave coastlines experience sea-breeze divergence (McPherson 1970). Similarly, Pielke (1974) and Boybeyi and Raman (1992) show strong convergence associated with convex coastlines of the Florida peninsula. Thus, it seems likely that coastline irregularity strongly affects the location of precipitation. Because the area of surface convergence strongly determines the total rainfall amount (Ulanski and Garstang 1978), coastline curvature also may be a primary factor in determining rainfall intensity.

The influence of the mean wind on sea-breeze development has been well documented. Stronger convergence occurs when low-level prevailing winds oppose the sea breeze; weaker convergence occurs when low-level winds flow in the same direction as the sea breeze (Pielke 1974; Boybeyi and Raman 1992; Atkins and Wakimoto 1997). The role of mesoscale variations in wind has received less attention. Heterogeneous initial conditions often produce better simulations in mesoscale models (e.g., Nair et al. 1997), implying that mesoscale variations play an important role in storm development. Thus, the presence of a well-developed early-morning land breeze (i.e., mesoscale variation in wind) may modify the location and strength of subsequent sea-breeze convergence zones and therefore may affect the location and intensity of precipitation.

To assess the relative importance of these factors on sea-breeze-initiated precipitation, we conduct idealized numerical simulations of summertime Florida convection. A three-dimensional cloud-resolving model coupled with a sophisticated land surface model is used to test the sensitivity of sea-breeze-initiated precipitation to initial soil moisture distribution, coastline irregularities, and initial wind distribution. The impact of Lake Okeechobee on timing, location, and intensity of precipitation is also considered. The next section presents representative Florida convective development with prevailing westerly winds. Section 3 introduces the coupled atmosphere–land surface model, and section 4 describes results from model simulations. Implications of these results for Florida precipitation, land surface–atmosphere interaction, and numerical weather prediction are presented in the discussion.

2. Characteristic Florida convection

A typical summertime convective line developed over central Florida on 27 July 1991 during the Convection and Precipitation Electrification Experiment (CaPE). This day illustrates the characteristic evolution of sea-breeze convergence and convective development over Florida with westerly winds (Halverson et al. 1996; Wilson and Megenhardt 1997). In the discussion below, all times will be given in local standard time (LST) because of the diurnal nature of sea-breeze-initiated convection (UTC is 5 hours ahead of LST). Sea breezes developed along both coasts of central Florida, with the west-coast sea breeze (WCSB) penetrating farther into the peninsula interior than did the east-coast sea breeze (ECSB). Westerly low-level winds (Fig. 1) produced this pattern by enhancing inward propagation of the WCSB and opposing inward penetration of the ECSB. By 1300 LST, convective cells developed along the WCSB front (Fig. 2a). The WCSB front continued to propagate farther inland, and the western half of central Florida was covered by convective clouds by 1500 LST. Clouds along the ECSB front were beginning to develop by this time (Fig. 2b). Cold outflow from WCSB convective cells collided with the ECSB front (Wilson and Megenhardt 1997), and a well-developed squall line occurred along the east coast by 1700 LST (Fig. 2c). The squall line first developed just after 1500 LST and began to dissipate at roughly 1800 LST (Halverson et al. 1996). This pattern of convective development is characteristic of type-3 Florida convection in which a strong north–south line of echoes develops along the east coast in response

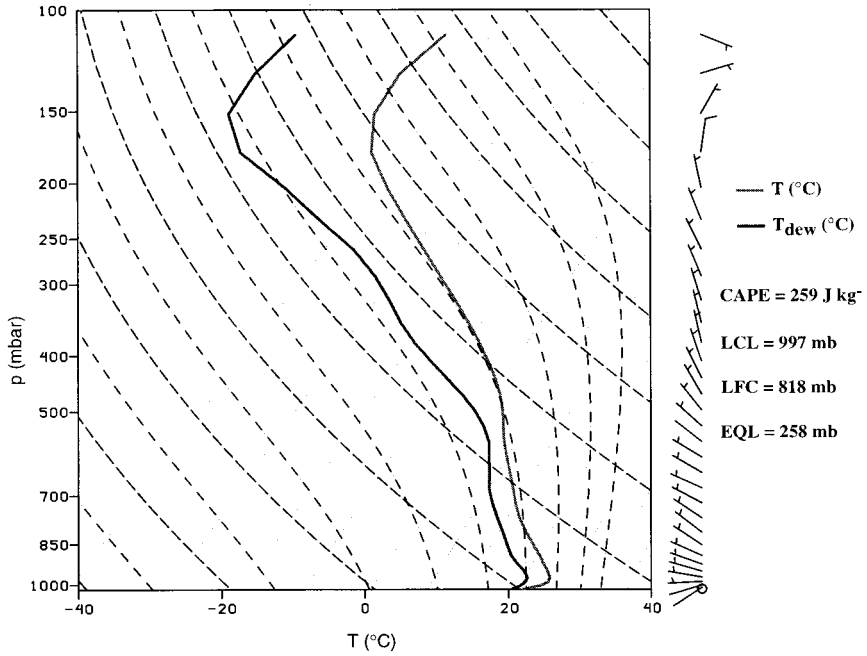

FIG. 1. Average sounding from four sounding locations in central Florida (Tampa, Dunnellon, Daytona, and Fellsmere) 0600 LST (1100 UTC) 27 Jul 1991.

to a merger of the WCSB and the ECSB (Blanchard and Lopez 1985).

Figure 3 shows observed accumulated rainfall on 27 July 1991 from 0600 to 2100 LST collected by rain gauges from CaPE Portable Automated Mesonet (PAM) stations and National Oceanic and Atmospheric Administration (NOAA) weather stations. The CaPE network comprised a dense array of observing stations in east-central Florida, and the NOAA sites are more evenly (and sparsely) distributed throughout the peninsula. Further details on the observational network during CaPE can be found in Halverson et al. (1996). Barnes objective analysis with a 30-km radius of influence and 25 iterations is used to interpolate between stations. Because two networks with very different spacing are used to produce the precipitation map, sensitivity analyses were performed to assess the impact of radius of influence on precipitation distribution. The interpolated values near NOAA sites were largely insensitive to the radius of influence. However, the PAM sites with fine spatial resolution produced overly smooth values (lower peaks) of precipitation with radii greater than 50 km. A radius of influence of 30 km produced a balance between smooth interpolation of the two datasets and conservation of peak values. As Fig. 3 indicates, relatively weak rainfall (0–25 mm) associated with WCSB convection occurred over west-central Florida. Larger rainfall amounts occurred over east-central Florida, with strong rainfall peaks of 53–62 mm. Rainfall in eastern Florida on this day was associated with the late-afternoon squall line. Radar images (not shown) with strong cells of over 50 dBZ in eastern Florida confirm the distribution of rainfall measured by rain gauges (Halverson et al. 1996).

3. Model

a. GCE–PLACE

The purpose of this paper is to isolate physical processes that contribute to timing, intensity, and location of diurnal precipitation in central Florida. To accomplish this goal, we utilize the GCE–PLACE coupled atmosphere–land surface model. The atmospheric model is the three-dimensional Goddard Cumulus Ensemble (GCE) cloud-resolving model (Tao and Simpson 1993). The GCE cloud model is a high-resolution, anelastic, nonhydrostatic model that has been extensively applied to study cloud–environment interaction, cloud mergers, air–sea interaction, cloud–radiation interaction, and trace gas transport (e.g., Simpson and Tao 1993). The model includes solar and infrared radiative transfer processes, a Kessler two-category liquid water scheme, and three-category ice microphysics schemes (Lin et al. 1983; Rutledge and Hobbs 1984). The Rutledge–Hobbs microphysics scheme is utilized in this study given the tropical characteristics of the sounding (Fig. 1). GCE is an active participant in the Global Energy and Water Cycle Experiment Cloud System Study cloud-resolving model intercomparison project (Moncrieff et al. 1997). Halverson et al. (1996) used a two-dimensional version of GCE (without the land surface model) to assess heating rates associated with the 27 July 1991 Florida squall line.

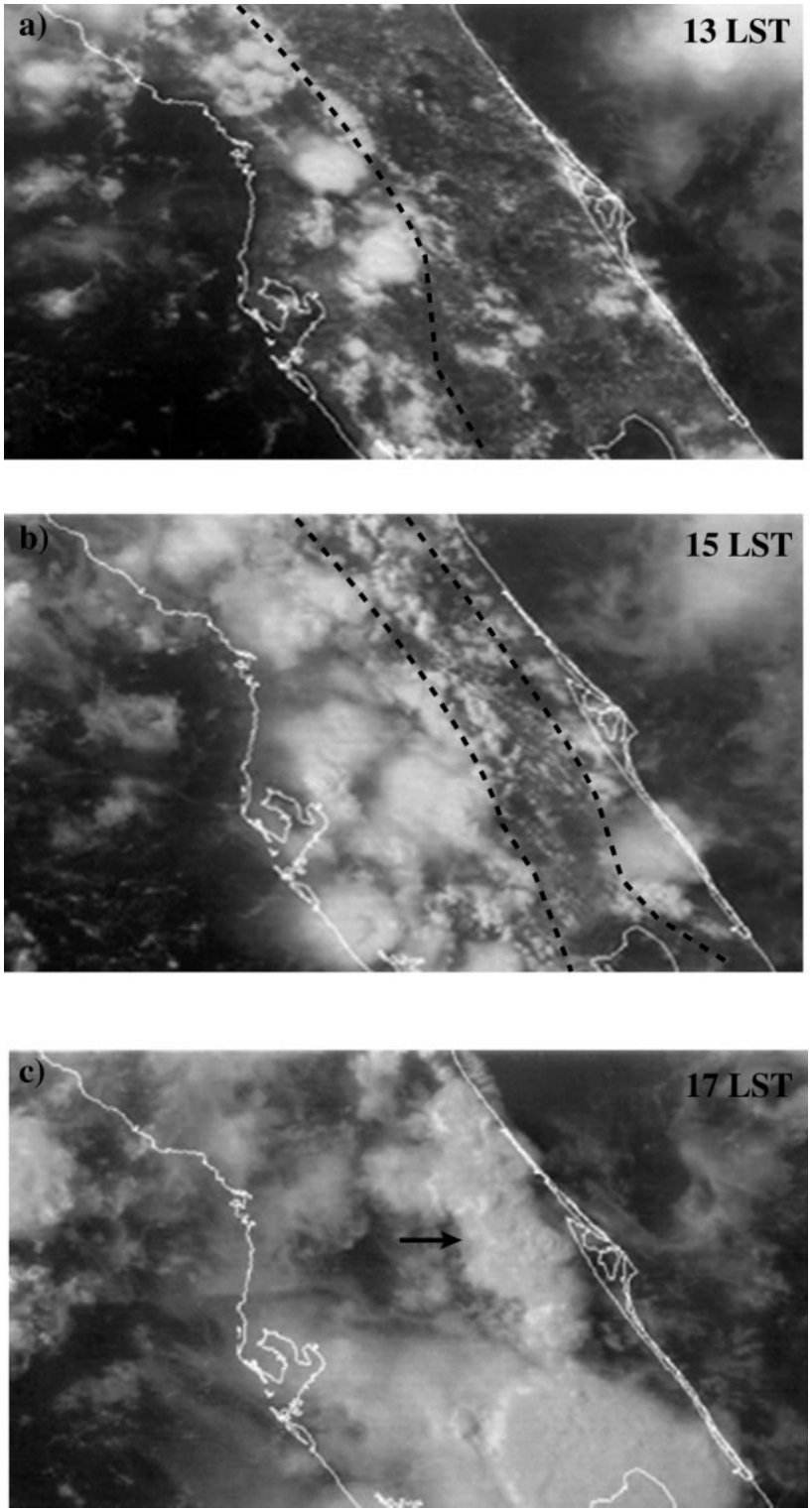

FIG. 2. *GOES-7* 1-km visible satellite images over central Florida on 27 Jul 1991 at (a) 1301 LST (1801 UTC), (b) 1501 LST (2001 UTC), and (c) 1701 LST (2201 UTC). Dashed lines indicate sea-breeze fronts, and the arrow indicates squall line location.

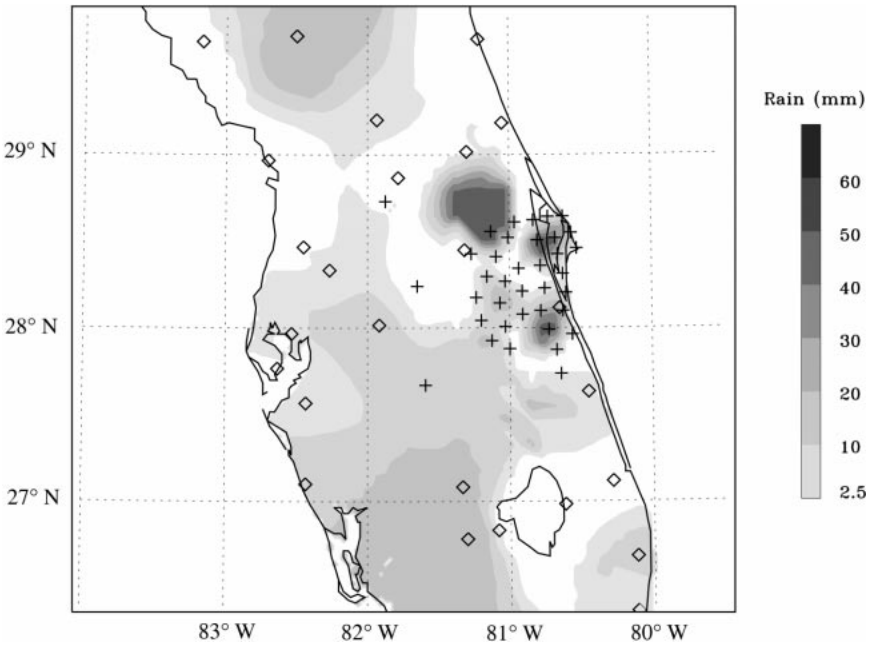

FIG. 3. Accumulated rainfall, 0600–2100 LST 27 Jul 1991, from rain gauge measurements. Crosses indicate PAM site locations and diamonds indicate NOAA weather observing sites.

The land surface component of GCE–PLACE is the Goddard Parameterization for Land–Atmosphere–Cloud Exchange (PLACE; Wetzel and Boone 1995). PLACE provides state-of-the-art representation of land surface processes. The land surface water budget incorporates precipitation, evapotranspiration, plant uptake, infiltration, and runoff. Soil temperatures evolve through an imbalance of surface net radiation, ground heat flux, sensible heat flux, and latent heat flux. Momentum, sensible heat, and latent heat fluxes are calculated using similarity relationships (Businger et al. 1971; Zilitinkevich 1975). The soil component includes five soil layers for soil moisture and seven soil layers for soil temperature. The additional two layers for soil temperature are needed to resolve large temperature gradients near the surface. Vegetation is represented by a single layer. Eight different soil types and fourteen different vegetation types may be selected. PLACE is a participant in the Project for Intercomparison of Land Surface Parameterization Schemes (Chen et al. 1997).

The atmospheric component of GCE–PLACE provides surface winds, surface air temperature, surface pressure, atmospheric moisture, shortwave and longwave radiation, and precipitation to the land surface. The land surface component returns momentum, sensible heat, and latent heat fluxes to the atmosphere. The coupling is two-way interactive. For example, precipitation can alter the distribution of soil moisture, which in turn changes the partitioning of energy between sensible heat and latent heat. These heat fluxes then feed back on subsequent development of clouds and precipitation. A two-dimensional version of GCE–PLACE has previously been used to investigate landscape-generated deep convection (Lynn et al. 1998).

TABLE 1. Model simulations.

Case	Coastline	Initial condition	
		Soil moisture	Wind
SAA	Straight	Average	Average
SVA	Straight	Variable	Average
SAV	Straight	Average	Variable
SVV	Straight	Variable	Variable
CAA	Curved	Average	Average
CVA	Curved	Variable	Average
CAV	Curved	Average	Variable
CVV	Curved	Variable	Variable
CVVOkee	Curved	Variable	Variable

b. Experimental design

Idealized numerical experiments (Table 1) are performed to test the sensitivity of sea-breeze-initiated precipitation to soil moisture, coastline curvature, and land breezes. The main purpose here is to isolate the effect of these factors on precipitation rather than to reproduce observations exactly. However, as described in more detail below, all simulations reproduce the general evolution of the 27 July 1991 storm, indicating that our idealized simulations capture much of the essential physics responsible for diurnal precipitation over Florida. Each simulation is labeled by three letters: the first letter documents a straight (S) or curved (C) coastline configuration, the second letter documents an average

(A) or variable (V) soil moisture initial condition, and the third letter represents average (A) or variable (V) initial winds. To first order, SAA can be viewed as the simulation that isolates the influence of average sea breezes on precipitation; the other simulations consider factors that may modulate sea-breeze evolution and subsequent precipitation. The domain size for each simulation is 400 km in the east–west direction, 400 km in the north–south direction, and 21 km vertically. The horizontal grid spacing is 3.1 km. Horizontal spacings of less than or equal to 4 km have been shown to capture squall-line dynamics sufficiently (Weisman et al. 1997). A stretched vertical grid with 80-m spacing at the surface and 1200-m spacing near the tropopause is implemented. Currently, the 3D GCE–PLACE model requires periodic horizontal boundary conditions. A 3D version with open boundary conditions is under development. Periodic boundary conditions are not overly restrictive in this case, given that local sea breezes are the primary forcing mechanism for precipitation on this day. The Florida coastline has been tilted horizontally in these simulations to insure periodic integrity in the north–south direction. If the southeast-to-northwest tilt of Florida were maintained in the simulations, land at the northern part of the domain would intersect ocean in the southern part of the domain. This alignment would produce unrealistic ''sea-breeze'' circulations near the boundaries. A sponge layer exists in the upper 5 km of the experimental domain to absorb vertically propagating internal gravity waves. Each simulation is integrated for 15 h from 0600 to 2100 LST with a time step of 5 s.

Four numerical experiments consider a simplified, straight coastline (Fig. 4a). The peninsular width in these simulations is 200 km, with 100 km of ocean on each side. The other experiments consider a Florida-like curved coastline with the peninsular width varying from 160 to 220 km (Fig. 4b). The first eight simulations do not include Lake Okeechobee in the south-central part of the domain. However, significant lake breezes may develop in response to differential heating near Lake Okeechobee (Pielke 1974; Boybeyi and Raman 1992). Indeed, a large convective cell likely associated with a lake breeze formed northwest of Lake Okeechobee on 27 July 1991 (Fig. 2). To test the effect of Lake Okeechobee on precipitation, an additional experiment (CVVOkee) has been performed.

Table 2 provides the land surface characteristics for the GCE–PLACE simulations. A sandy clay loam soil type and tall broadleaf trees with ground cover are used in this study. Land surface characteristics such as surface roughness, surface albedo, fractional vegetation cover, and leaf area index are derived from International Satellite Land Surface Climatology Project data (Meeson et al. 1995). Normal distributions of these quantities (average values and standard deviations are provided in Table 2) for the selected soil texture, vegetation type, and month are used to account for surface heterogeneity. The total soil depth is 3m, with soil-layer thicknesses ranging from 1 cm at the top to 2 m at the bottom.

c. Initial conditions

The key differences among the numerical experiments (Table 1) are different initial conditions at 0600 LST and different lower boundary conditions (straight coastline vs curved coastline). In all cases, the initial thermodynamic and moisture sounding (Fig. 1) is an average sounding from four locations: Tampa and Dunnellon on the west coast, and Daytona Beach and Fellsmere on the east coast. A relatively low value for convectively available potential energy (CAPE) of 259 J kg^{-1} initially occurs. Naturally, CAPE will increase throughout the day as the land surface warms and moistens the atmosphere above.

Offline PLACE simulations provide the initial distribution of soil moisture. The initial value of soil moisture in the offline PLACE calculations is 0.3 $cm^3\ cm^{-3}$ (75% of soil porosity). Observed precipitation of the previous 6 days is input into PLACE, and new values of soil moisture are returned. Given the uncertainty of the soil moisture originally input into offline PLACE, the new values of soil moisture are used as initial conditions for another offline PLACE calculation. This process is repeated until the soil moisture distribution achieves steady state (50 iterations are used here). Figure 4 shows soil moisture distribution in the root zone (5–100-cm depth) used in simulations with initially varying soil moisture (SVA, SVV, CVA, CVV, and CVVOkee). Root zone soil moisture is shown, because the root zone largely determines moisture availability over vegetated surfaces. Lake Okeechobee is only present in the case of CVVOkee. Two relatively wet strips of land exist within the peninsula: one oriented in the east–west direction at roughly $y = 320$ km and the other oriented in the northwest–southeast direction over east-central Florida. Dry patches of land exist in west-central Florida from $y = 30$ to $y = 250$ km and east of Lake Okeechobee. Simulations SAA, SAV, CAA, and CAV use the horizontally averaged value of PLACE-derived soil moisture in each soil layer (the root zone average soil moisture is 0.22 $cm^3\ cm^{-3}$). Random perturbations in soil moisture ($\pm 0.01\ cm^3\ cm^{-3}$) are applied throughout the peninsula in all simulations to promote convective development.

Figure 5 shows initial surface winds (minus the domain averaged value of 3.2 m s^{-1}) for experiments with variable initial horizontal wind (SAV, SVV, CAV, CVV, and CVVOkee). The distribution of wind in Fig. 5 has been interpolated from wind measurements from the four sounding sites. Winds vary horizontally at all heights, but only the surface winds are shown in Fig. 5. Moderate land breezes with wind speeds of approximately 2 m s^{-1} occur along both coasts. The wind distribution for simulations CAV, CVV, and CVVOkee (curved coastline) is identical to the wind distribution for simulations SAV and SVV (straight coastline). Sim-

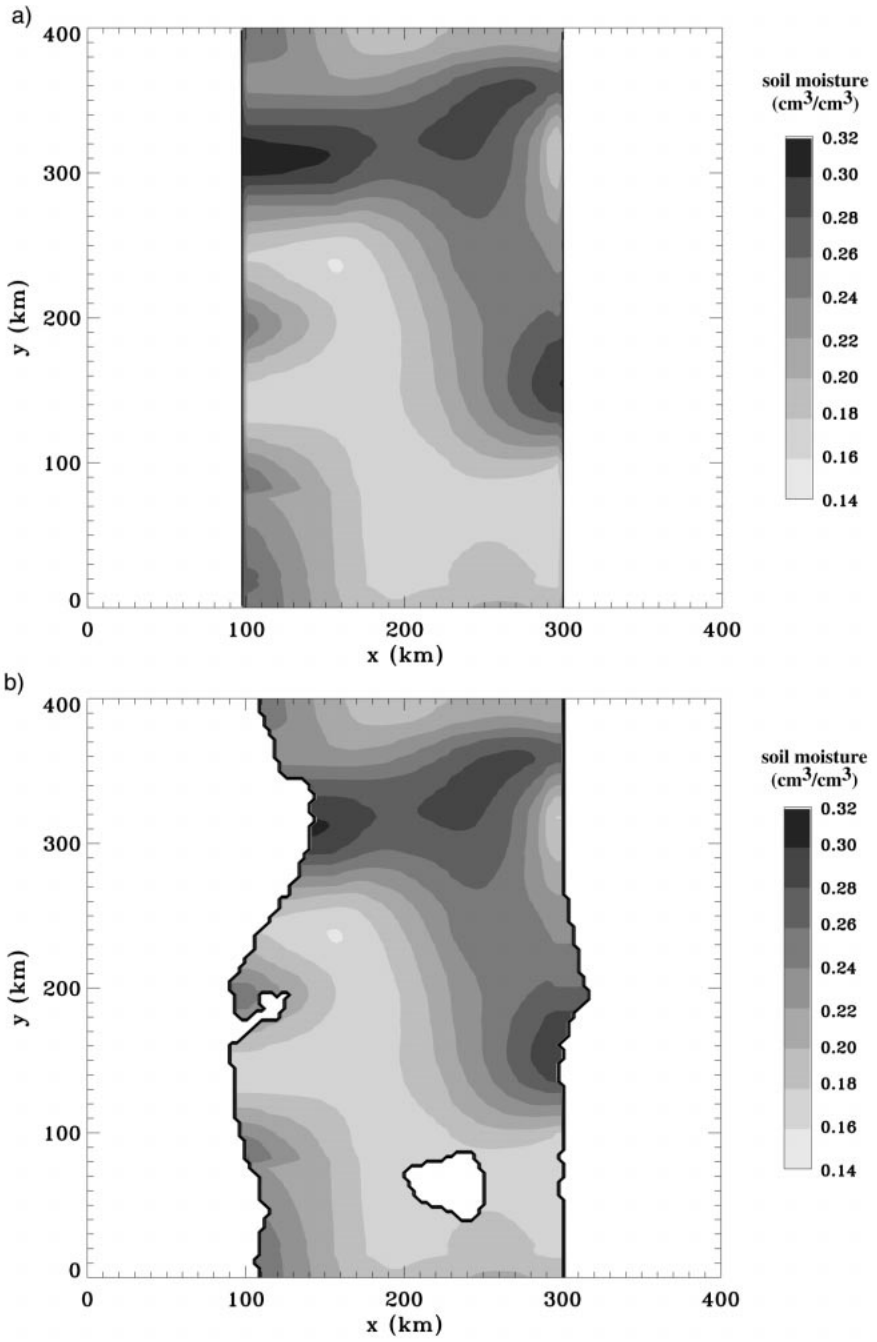

FIG. 4. Initial root zone soil moisture derived from offline PLACE simulations for 0600 LST 27 Jul 1991 for (a) straight coastline simulations with variable initial soil moisture (cases SVA and SVV) and (b) curved coastline simulations with variable initial soil moisture (cases CVA, CVV, and CVVOkee). Only CVVOkee includes Lake Okeechobee. SAA and SAV use the straight coastline configuration with horizontally averaged initial soil moisture; CAA and CAV use the curved coastline configuration with average initial soil moisture.

ulations SAA, SVA, CAA, and CVA use a homogeneous distribution of horizontal wind, the average from the four soundings (Fig. 1).

The initial soil temperature is derived from offline PLACE simulations and then is horizontally averaged in each of the seven soil temperature layers. The initial surface temperature over land at 0600 LST is 301.1 K. The initial average sea surface temperature (301.7 K) for 27 July 1991 is obtained from the Comprehensive Ocean–Atmosphere Dataset (Woodruff et al. 1993).

TABLE 2. Land surface characteristics.

Characteristic	Value	Std dev
Soil texture	Sandy clay loam	
Vegetation	Tall broadleaf trees with ground cover	
Soil depth (m)	3.0	
Root zone depth (m)	1.0	
Wilting point ($cm^3\ cm^{-3}$)	0.144	
Porosity ($cm^3\ cm^{-3}$)	0.404	
Surface roughness (m)	0.25	0.13
Albedo	0.1869	0.0186
Fractional vegetation	0.4297	0.1972
Leaf area index	1.29	0.74

PLACE treats the ocean as static layers of water with no horizontal transport (i.e., no dynamics). The sea surface temperature evolves throughout the simulations but remains close to the initial value.

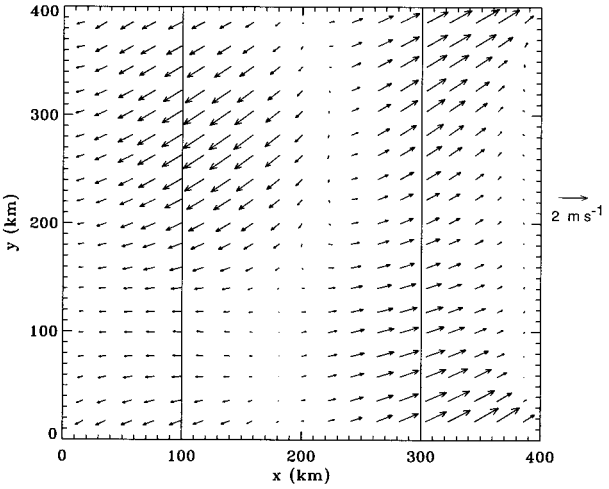

FIG. 5. Initial surface winds for simulations with horizontally varying initial winds (SAV, SVV, CAV, CVV, and CVVOkee). Land breezes can be seen along both coasts.

4. Results

a. General evolution: Timing, location, and intensity

All model simulations reproduce the general evolution of sea-breeze-initiated clouds and precipitation over Florida on 27 July 1991. Figure 6 shows the vertically integrated hydrometeor (cloud water, rain, ice, snow, and graupel) mass per unit area for simulation CVV at 1300, 1500 and 1700 LST. Evolution of total hydrometeors in simulation CVV agrees qualitatively with the observed cloud evolution (Fig. 2). At 1300 LST, strong convective cells have developed in simulation CVV along the west coast associated with the west-coast seabreeze front. Smaller clouds have also formed along the east coast, consistent with satellite observations. By 1500 LST, west-coast convection cells have become larger, and east-coast convection cells are more numerous. At 1700 LST, a line of cells has developed along the east coast, and cloud coverage on the western half of the peninsula has diminished. The other simulations show similar evolution; specific differences among the simulations will be addressed below.

The impact of the three factors (soil moisture, coastline curvature, and land breezes) on the location and intensity of precipitation can be assessed from accumulated rainfall maps. Figures 7 and 8 show the accumulated rainfall from 0600 to 2100 LST for straight coastline and curved coastline simulations, respectively. [The simulation with Lake Okeechobee (CVVOkee) will be discussed later.] All cases reproduce the general pattern of precipitation, with relatively low rainfall amounts on the western half of the peninsula and stronger precipitation on the eastern half. The location of heaviest precipitation in control simulation SAA occurs in the northeastern part of the peninsula ($x = 260$ km, $y = 290$ km). A different random perturbation in initial soil moisture would likely have produced a different distribution. However, all simulations used the same random perturbation in soil moisture, so differences among the simulations cannot be attributed to these random perturbations.

In all simulations but SAV, the location of maximum accumulated precipitation is significantly altered. Here, we use the somewhat arbitrary value of 75 km to assess differences in location. The change in location is considered to be significant if the location of peak precipitation differs by more than 75 km. If the criterion were lowered to 50 km, all simulations would exhibit significant location differences; if the criterion were raised to 100 km, only simulations CAA and CAV would show significant location changes. Simulations with variable soil moisture (SVA, SVV, CVA, and CVV) all show the highest peak rainfall in the northern part of the domain where soil moisture is abundant. In addition, simulations with coastline curvature show increased rainfall over Cape Canaveral when compared with control simulation SAA, suggesting that coastline curvature is instrumental in determining the location of heavy precipitation. Last, unlike all other simulations, case CAV shows heaviest precipitation in the southern part of the domain, suggesting that coastline curvature and land breezes together can significantly modify the location of heavy rainfall.

Soil moisture and coastline curvature together strongly influence the intensity of precipitation. Simulations CVA and CVV exhibit the largest peak rainfall amounts (67.3 and 65.9 mm as compared with 47.0 mm for simulation SAA). Interestingly, soil moisture or coastline curvature alone cannot account for these large peak accumulations. For example, simulations with variable soil moisture but straight coastlines produce peak rainfall amounts comparable to control simulation SAA (49.7 and 47.6 mm for SVA and SVV, respectively). Likewise, CAA (coastline curvature) produces a peak accumulation of only 45.1 mm.

Coastline curvature and land breezes influence the

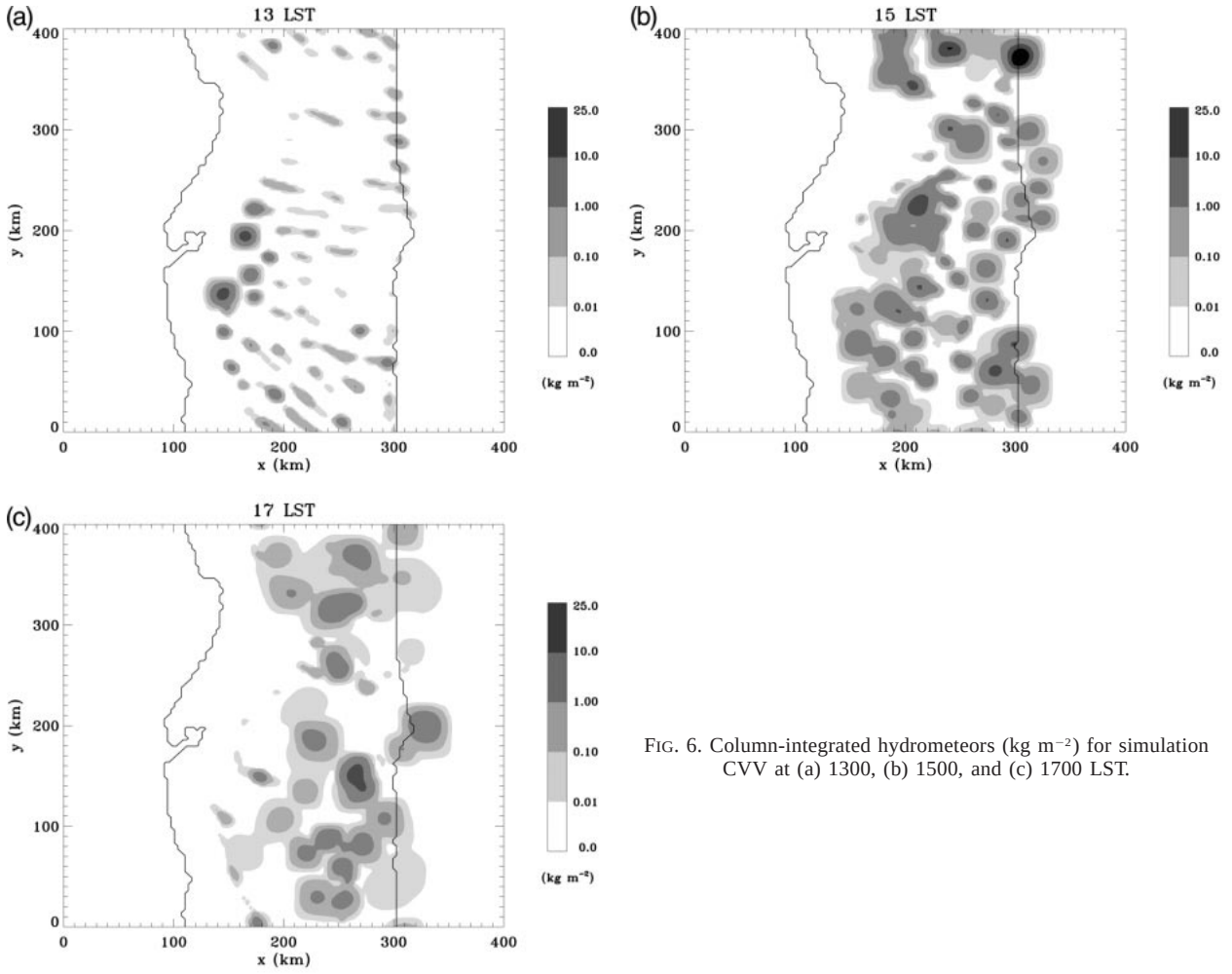

FIG. 6. Column-integrated hydrometeors (kg m^{-2}) for simulation CVV at (a) 1300, (b) 1500, and (c) 1700 LST.

timing of precipitation. Figure 9 plots the peak rain rate versus time for all simulations. The peak rain rate is defined as the maximum rain rate in the domain at a given time. All cases reproduce the diurnal evolution of sea-breeze-initiated precipitation over Florida. Precipitation begins around noontime, reaches peak values in the afternoon, and rapidly decays in the early evening. Significant differences can be seen among the simulations. Simulations with curved coastlines (except CVVOkee) produce the highest peak rain rates roughly 1 hour earlier than SAA. The presence of early-morning land breezes also affects the timing of peak precipitation. Similar to the curved coastline cases, simulation SAV exhibits maximum peak rain rates 1 hour earlier than other straight coastline cases.

With the exception of cases CVA and CVV, the maximum peak rain rate (which occurs in the afternoon) for the simulations is within a few percent of the SAA maximum peak rain rate (Fig. 9). Simulations CVA and CVV produce significantly higher maximum peak rain rates, with values 26% and 18% higher than SAA values, respectively. This result suggests that interplay between coastline curvature and soil moisture can produce significantly higher rain rates than do coastline curvature or soil moisture distribution alone, consistent with the peak accumulated rainfall results.

Table 3 provides a summary on the impact of soil moisture, coastline curvature, and land-breeze circulations on the timing, location, and intensity of precipitation. Simulation SAA is considered to be the control simulation with which other simulations are compared; it captures the first-order effect of average sea breezes on precipitation. Each factor is considered to be a significant influence if it alters the timing of precipitation by at least 1 hour, the location of maximum accumulated precipitation by at least 75 km, the peak rain rate by at least 5 mm h^{-1} (~15% of the maximum), and the accumulated rainfall by at least 7 mm (~15% of the peak accumulated rainfall in control simulation SAA). Soil moisture influences the location and intensity of precipitation. Coastline curvature largely influences the timing, intensity, and location of precipitation. Land breezes affect the timing of precipitation and may influence location in concert with coastline curvature. The

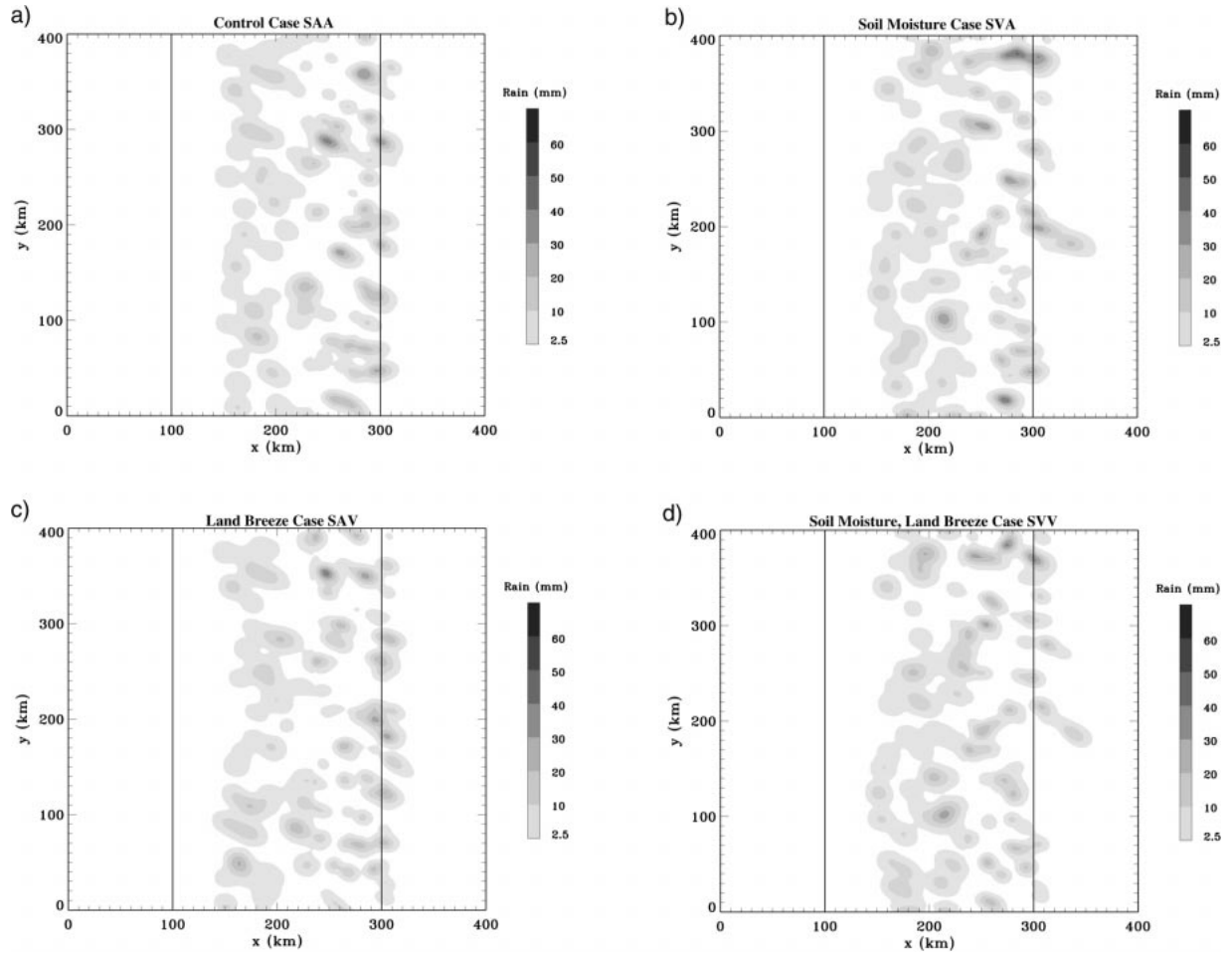

FIG. 7. Accumulated rainfall from 0600 to 2100 LST for simulations (a) SAA, (b) SVA, (c) SAV, and (d) SVV. See Table 1 for meaning of abbreviations.

physical mechanisms for modulating the timing, location, and intensity of precipitation by these factors are discussed below.

b. The role of soil moisture

Two possible causes for this interaction between soil moisture distribution and precipitation are mesoscale circulations induced by soil moisture gradients (e.g., Ookouchi et al. 1984; Yan and Anthes 1988; Lynn et al. 1998) and increased moisture in the convective boundary layer (Crook 1996; Eltahir 1998). There is some evidence of weak soil moisture–induced mesoscale circulations in our simulations. Figure 10 shows potential temperature and horizontal winds at 80 m above the surface at 1100 LST for simulations SAA and SVA. The horizontally averaged wind has been removed to delineate perturbations associated with mesoscale circulations. The sea breeze is well developed along both coasts in both simulations, while the peninsula interior is marked by small-scale perturbations associated with horizontal convective rolls. The major difference between SAA and SVA is reduced winds in the boundary layer in cool (wet) regions. For example, the sea-breeze circulation is significantly weaker at $x = 290$ km, $y = 160$ km and at $x = 120$ km, $y = 320$ km in simulation SVA than in SAA. At 80-m altitude, soil moisture–induced mesoscale circulations would be characterized by flow from cool (wet) regions to warm (dry) regions. There does appear to be enhanced flow in the central part of the peninsula southward from the cool region near $y = 320$ km to the warm region at $y = 150$ km. However, this circulation does not produce enhanced precipitation over the central part of the peninsula (Fig. 7). Instead, the largest peak occurs in the northern part of the peninsula near wet soil. Thus, mesoscale circulations produced by soil moisture gradients do not account for heavy precipitation in our simulations.

A more likely cause of enhanced precipitation is a moistened convective boundary layer over regions with wet soil. Figure 11 shows vertical slices of water vapor perturbation (total water vapor mixing ratio minus the horizontally averaged water vapor mixing ratio) below 1-km altitude at $y = 340$ km for simulations SAA and

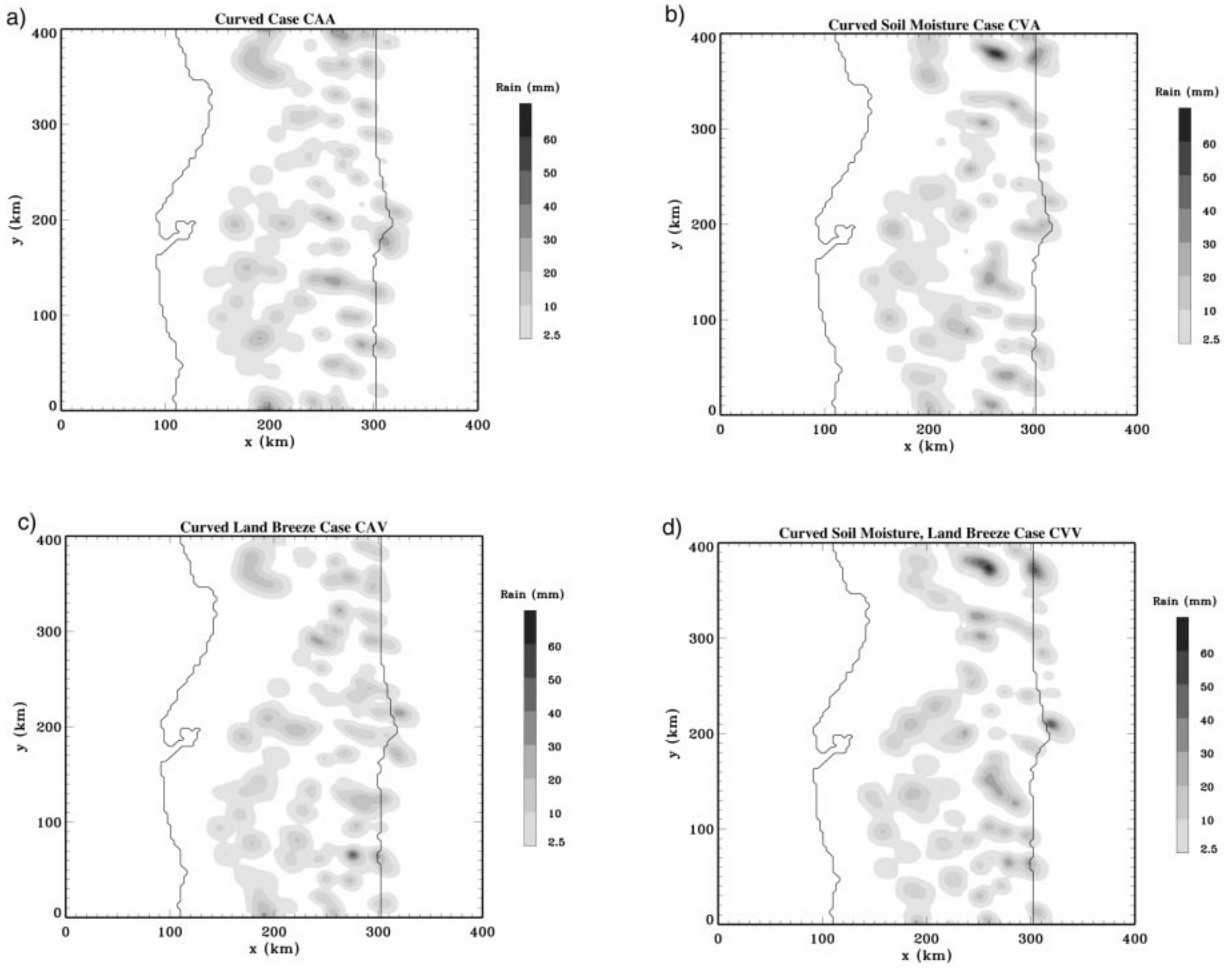

FIG. 8. Accumulated rainfall from 0600 to 2100 LST for simulations (a) CAA, (b) CVA, (c) CAV, and (d) CVV. See Table 1 for meaning of abbreviations.

SVA. The location at $y = 340$ km corresponds to large values of soil moisture in SVA (Fig. 4). At 1000 LST, the boundary layer over the peninsula in control simulation SAA shows water vapor perturbations of about 0.1–0.7 g kg^{-1} (Fig. 11). In contrast, the boundary over wet soil in simulation SVA shows water vapor perturbations of about 0.5–1.5 g kg^{-1}. Variations of boundary layer moisture of 1 g kg^{-1} can help to initiate moist convection in situations where deep moist convection is otherwise dormant (Crook 1996). CAPE, averaged over the peninsula at $y = 340$ km, is 14% larger in simulation SVA than in SAA. In addition, CAPE over wet soil ($y = 340$ km) is 21% larger than CAPE over dry soil ($y = 70$ km) in simulation SVA. The lifting condensation level (LCL) is also lower over wet soil in simulation SVA [950 hPa at $y = 340$ km (wet soil) vs 929 hPa at $y = 70$ km (dry soil)]. Thus, variations in soil moisture produce greater convective instability and a lower cloud base over regions with wet soil. Subsequent heavy precipitation falls near or downwind of these regions.

c. The role of coastline curvature

It is well established that coastline curvature affects sea-breeze convergence (e.g., McPherson 1970; Pielke 1974). Strong convergence occurs for coastlines with convex curvature while divergence occurs for concave coastlines. Vertical velocities are therefore larger inland of convex coastlines, and clouds preferentially develop at these locations (Pielke 1974; Simpson et al. 1980). This mechanism occurs in our simulations with curved coastlines. Figure 12 indicates the difference in low-level convergence for simulations CAA and SAA at 1000 LST in the lowest 440 m of the atmosphere. Strong convergence occurs in simulation CAA inland of convex coastlines (e.g., Tampa Bay peninsulas on the west coast and Cape Canaveral on the east coast). Low-level divergence occurs near concave coastlines (note strong divergence near Tampa Bay). By comparison, simulation SAA exhibits stronger convergence in regions where land has been replaced by water in CAA (e.g., $x = 120$ km, $y = 300$ km). In addition, peak values of

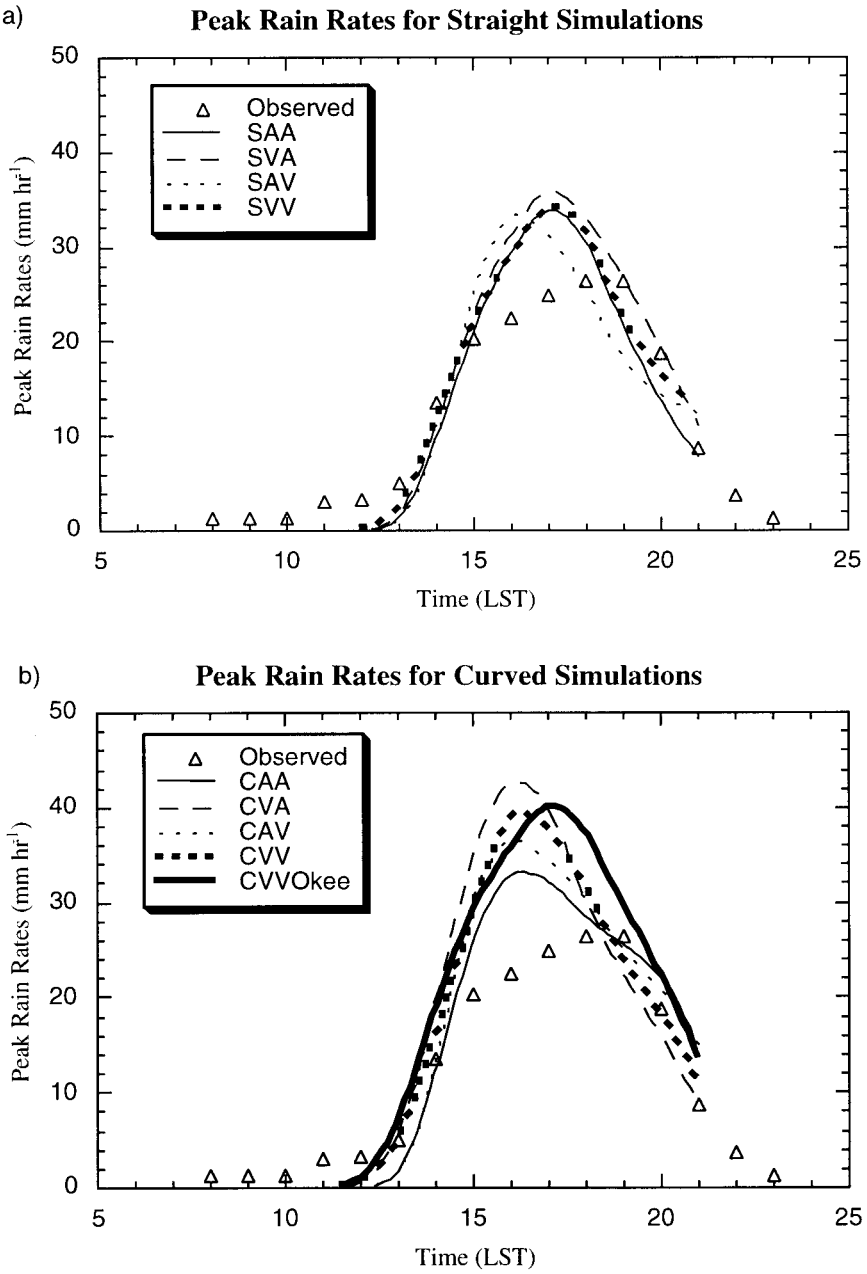

FIG. 9. Peak rain rates (mm h^{-1}) vs local time for (a) straight coastline simulations and (b) curved coastline simulations. Triangles indicate observed peak rain rates from rain gauge measurements.

convergence along the west coast are 28% larger in CAA than in SAA. Earlier strong low-level convergence due to convex coastlines likely accounts for earlier peak rainfall in the curved coastline simulations. Furthermore, the heaviest rainfall accumulations on the east coast roughly coincide with regions of strong convergence in the late morning.

d. The role of initial land breezes

It was believed prior to these simulations that the presence of land-breeze circulations (as opposed to horizontally homogeneous initial winds) would delay low-level convergence and precipitation, because sea-breeze development would have to overcome land-breeze circulations. Contrary to this hypothesis, land-breeze circulations cause earlier development of heavy precipitation in our simulations (Fig. 9). Figure 13 shows the difference map of low-level convergence between simulations SAV and SAA at 1000 LST. The presence of an early-morning land breeze inhibits convergence as expected only along the northeast coast [as shown by dashed lines (stronger convergence for SAA) in Fig.

TABLE 3. Summary of impact on precipitation by coastline curvature, soil moisture, land breezes, and Lake Okeechobee.

Factor (simulation)	Timing	Location	Intensity	
			Rain rate	Accumulation
Control (SAA)	–	–	–	–
Soil moisture (SVA)	–	X	–	–
Land breeze (SAV)	X	–	–	–
Soil moisture, land breeze (SVV)	–	X	–	–
Curved (CAA)	X	X	–	–
Curved, soil moisture (CVA)	X	X	X	X
Curved, land breeze (CAV)	X	X	–	–
Curved, soil moisture, land breeze (CVV)	X	X	X	X
Lake Okeechobee (CVVOkee vs CVV)	X	X	–	–

13]. Elsewhere along the coasts, stronger convergence occurs in the simulation with early-morning land breezes. In particular, the northwest quadrant of the peninsula exhibits substantially stronger convergence in simulation SAV. This convergence creates earlier cloud development and heavy rainfall in the northern part of the peninsula (Fig. 7).

e. Nonlinear interactions

Much of the impact on the timing, location, and intensity of precipitation (Table 3) can be attributed to a single factor (e.g., soil moisture or coastline curvature). For example, the location of heavy precipitation in simulations SVA and SVV coincides with initially wet soil. Likewise, timing and location changes in simulations with coastline curvature (CAA, CVA, CAV, and CVV) can be attributed to earlier low-level convergence near convex coastlines.

However, nonlinear interactions between the three factors (soil moisture, coastline curvature, and land breezes) do account for some of the differences among the simulations. Perhaps the most dramatic example of nonlinear interaction is detected in rainfall intensity. Simulation CVA (curvature and soil moisture) exhibits significantly larger peak accumulations (Fig. 8) and peak rain rates (Fig. 9) than simulations CAA (curvature only) and SVA (soil moisture only). Simulation CVV (all three factors present) shows similar behavior to CVA except that the maximum peak rain rate is slightly less. Indeed, peak accumulations occur at roughly the same location (near wet soil) in simulations SVA, SVV, CVA, and CVV, but the highest single values exist in the simulations with both coastline curvature and soil moisture variations. Thus, nonlinear interaction between soil moisture and coastline curvature accounts for the intense rainfall in simulations CVA and CVV.

Simulation CAV (curvature and land breeze) also exhibits a feature not present in simulations with either coastline curvature (CAA) or land breezes (SAV) alone. The largest accumulation of rainfall in CAV occurs in the southern part of the peninsula; all other simulations have peak accumulations in the central or northern part of the peninsula. The general pattern of low-level convergence in simulation CAV (not shown) does not differ significantly from simulation CAA. Instead, heavy precipitation in simulation CAV appears to result from isolated *local* convergence. The convective cloud associated with this rain event developed between two older clouds along the east-coast sea-breeze front, suggesting that the heavy accumulation is a result of strong convergence due to cold outflow boundaries of adjacent clouds (e.g., Simpson et al. 1980; Tao and Simpson 1989). This result underscores the extreme sensitivity of cloud development on initial winds and coastline curvature.

f. Lake Okeechobee

An additional simulation has been performed to assess the effect of Lake Okeechobee on timing, intensity, and location of precipitation. All three factors considered previously (coastline curvature, soil moisture, and land breezes) are present in the Lake Okeechobee simulation (CVVOkee). To isolate the effect of the lake, this simulation should be compared with simulation CVV rather than with simulation SAA as for the other simulations. As Fig. 4b indicates, Lake Okeechobee covers approximately 150 km^2, comparable in size to the wettest soil regions. Land surrounding the lake is very dry in this simulation, so lake breezes that are generated by temperature contrasts between land and water should be maximized. Figure 14 shows the accumulated rainfall for CVVOkee from 0600 to 2100 LST, and Fig. 9 plots the temporal evolution of peak rain rate. Heavy rainfall still occurs near the northern wet soil region and near Cape Canaveral, but the highest accumulated rainfall occurs northwest of Lake Okeechobee. In addition, the leeward (east) side of the lake experiences no rainfall (Fig. 14). This distribution is in rough agreement with observations (Fig. 3), although much heavier precipitation occurs northwest of the lake in the simulation. The maximum values of peak rain rate are similar between CVV and CVVOkee, but the peak is delayed by 1 hour in simulation CVVOkee (Fig. 9). Thus, Lake Okeechobee strongly influences the timing and location of precipitation but not the intensity (Table 3).

5. Discussion

Our model results confirm previous Florida simulations (e.g., Pielke 1974; Simpson et al. 1980; Boybeyi

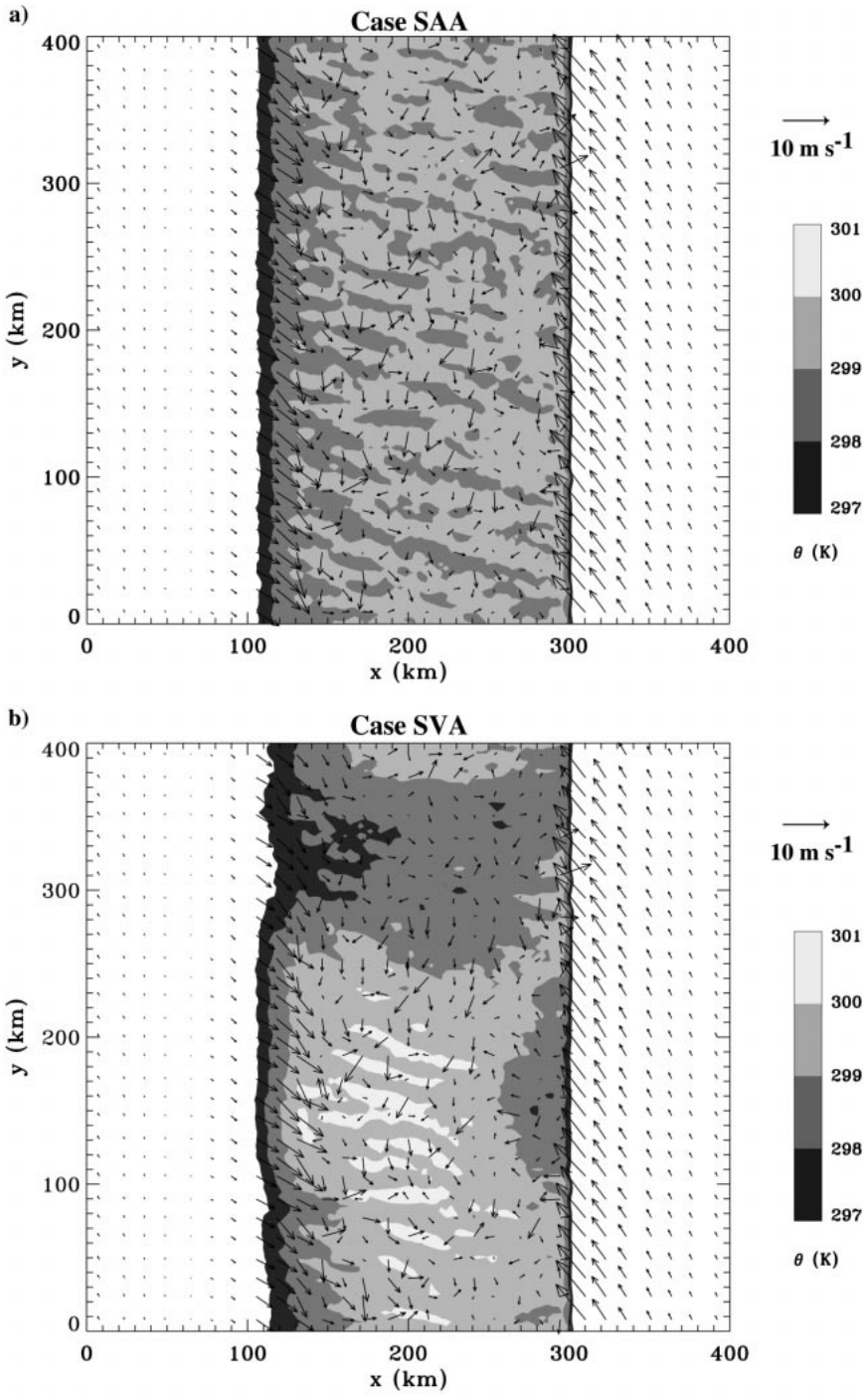

FIG. 10. Potential temperature θ (over land only) and perturbation horizontal winds at 80-m height at 1100 LST for (a) simulation SAA and (b) simulation SVA.

and Raman 1992) regarding the relationship of coastline curvature, low-level convergence, and cloud development. Our simulations provide strong evidence on the impact of coastline curvature by comparing simulations with straight coastlines and curved coastlines, an approach not considered in previous work. Simulations with curved coastlines qualitatively agree most closely with the observed location of heavy precipitation (i.e., near Cape Canaveral). Convex coastlines have long been known as preferred locations for cloud formation (Pielke 1974; Simpson et al. 1980; Boybeyi and Raman 1992).

However, soil moisture also has a dramatic impact on the spatial distribution of precipitation. Heavy rainfall preferentially occurs near or downwind of wet soil. The

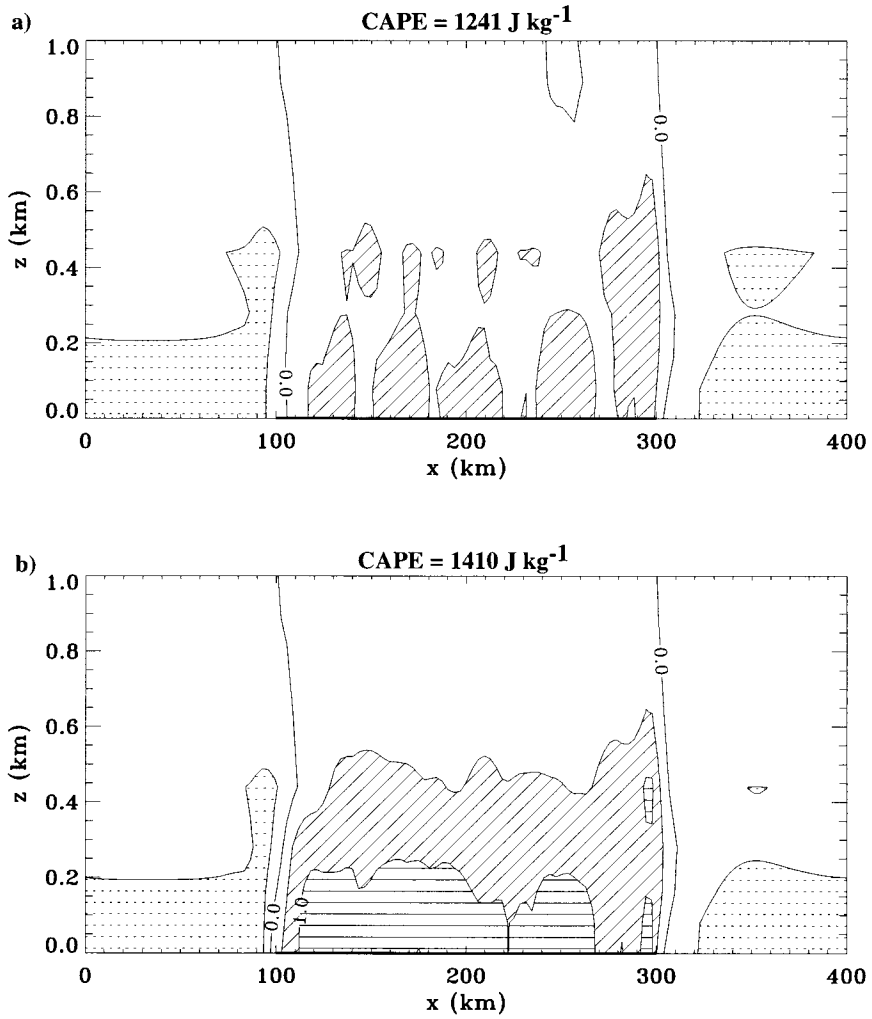

FIG. 11. Water vapor mixing ratio perturbation at $y = 340$ km in the lowest 1 km at 1000 LST for simulations (a) SAA and (b) SVA. The contour interval is 0.5 g kg^{-1}. Dashed lines indicate values less than -0.5 g kg^{-1}, slanted solid lines indicate values between 0.5 and 1.0 g kg^{-1}, and horizontal solid lines indicate values greater than 1.0 g kg^{-1}. CAPE averaged across the peninsula at $y = 340$ km is shown above the panels.

initial distribution of soil moisture in our model is determined from precipitation measurements over the previous six days. Numerous small lakes and rivers in central Florida are neglected in our simulations. For example, the Indian River in the Cape Canaveral area often exhibits a river-breeze circulation that interacts with the east-coast sea-breeze front (Rao et al. 1999). Inclusion of inland water bodies in our model would increase the ''effective'' soil moisture in east-central Florida and possibly would help to account for heavy precipitation observed inland of Cape Canaveral.

As compared with previous Florida simulations, our simulations provide an alternative view regarding the role of soil moisture. Xu et al. (1996) find that their wet soil simulation produces peak accumulated rainfall amounts *less* than those in their dry soil simulation, implying that large values of soil moisture inhibit sea-breeze-initiated precipitation. Our results suggest the opposite: soil moisture can promote convective development and subsequent precipitation. Soil moisture in our simulations acts as an atmospheric moisture source, thereby increasing CAPE and preferentially producing heavy rainfall over previously wet soil. A positive feedback mechanism may begin in which rainfall increases soil moisture which, in turn, promotes heavy rainfall in the same location. The positive feedback mechanism between soil moisture and precipitation has been observed in many observational and numerical studies (e.g., Segal et al. 1995; Clark and Arritt 1995; Beljaars et al. 1996; Findell and Eltahir 1997; Taylor et al. 1997; Eltahir 1998). A key prerequisite for this positive feedback is a moist atmosphere. In our simulations, relative humidities of roughly 80%–85% exist initially at 0600 LST from the surface to 500 hPa. The atmosphere is

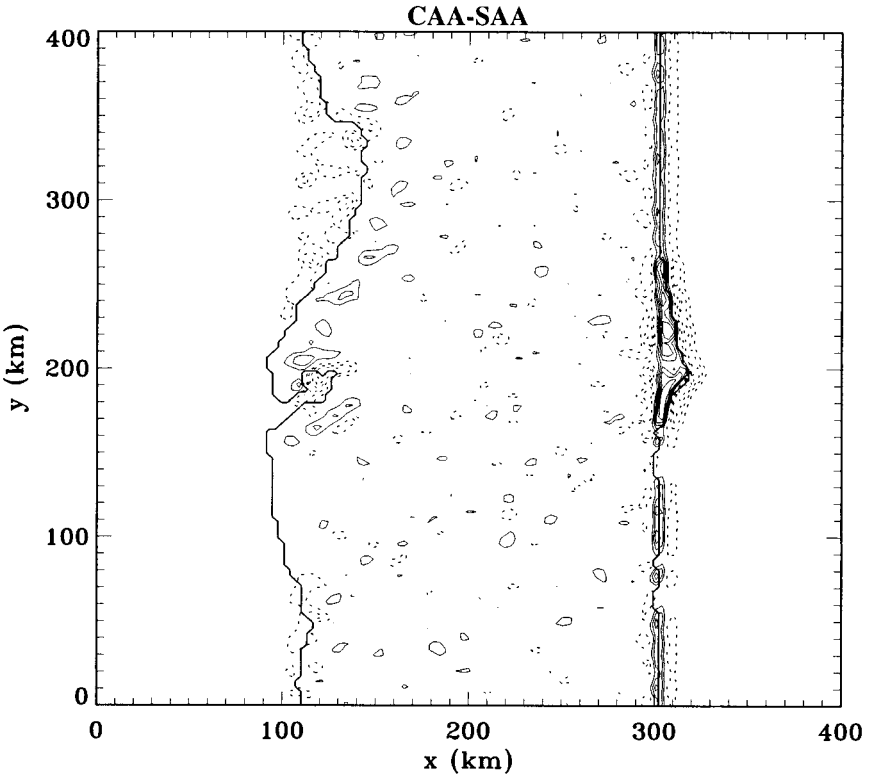

FIG. 12. Difference in low-level convergence below 440-m altitude at 1000 LST between simulations CAA and SAA. Solid contour lines indicate stronger convergence for CAA, and dotted lines indicate stronger convergence for SAA. The contour interval is 0.0003 s^{-1}.

primed to convect under these moist conditions, and soil moisture gives the atmosphere a boost toward convective instability. If the atmosphere were relatively dry, large values of soil moisture would reduce the sensible heat flux to the atmosphere and would likely inhibit convective development. In fact, the atmospheric sounding used in Xu et al. (1996) is significantly drier than the sounding used here. The ability of soil moisture to influence convective development may be intimately tied to existing atmospheric moisture conditions (e.g., Rabin et al. 1990).

Mesoscale circulations induced by soil moisture gradients are present in our simulations, but they have little impact on the development of heavy precipitation. Existing atmospheric conditions may also regulate the impact of soil moisture–induced circulations on rainfall. Drier atmospheric conditions would result in a higher LCL, thus requiring stronger uplift (perhaps produced by soil moisture–induced circulations) to produce clouds and rain. Furthermore, strong mesoscale circulations are characteristically found in numerical simulations with relatively weak environmental winds and stepwise soil moisture gradients (e.g., Yan and Anthes 1988; Avissar and Liu 1996; Lynn et al. 1998). Although initial low-level wind shear in our simulations (4.3 m s^{-1} from the surface to 1-km altitude) is relatively weak, environmental winds of roughly 3–5 m s^{-1} in the boundary layer may be large enough to disrupt mesoscale circulations induced by soil moisture. Soil moisture gradients in our simulations are much smoother than stepwise gradients in previous idealized simulations, perhaps further inhibiting development of strong mesoscale circulations. Indeed, the sharp gradient of ''soil moisture'' produced by Lake Okeechobee does result in strong mesoscale circulations (lake breezes) and heavy precipitation.

Although the model performs very well in capturing sea-breeze development, cloud formation, cloud propagation, and convective precipitation, it does a lesser job of producing a broad stratiform region behind the line of convective cells. As a result, the area-averaged rain rates in all simulations (not shown) are roughly 40%–50% of observed area-averaged rain rates. One possible reason for the development of a weak squall line in our simulations is the presence of weak low-level shear. Cloud models often have difficulty producing strong squall lines under weakly sheared conditions (e.g., Rotunno et al. 1988). In addition, squall line simulations without artificial cool pool initiation may require very fine horizontal grid resolution of 1 km or less to capture cloud mergers adequately (Tao and Simpson 1989). Improvements in cloud microphysics from a three-ice scheme to a four-ice scheme (Ferrier et al. 1995) may result in better simulation of trailing strati-

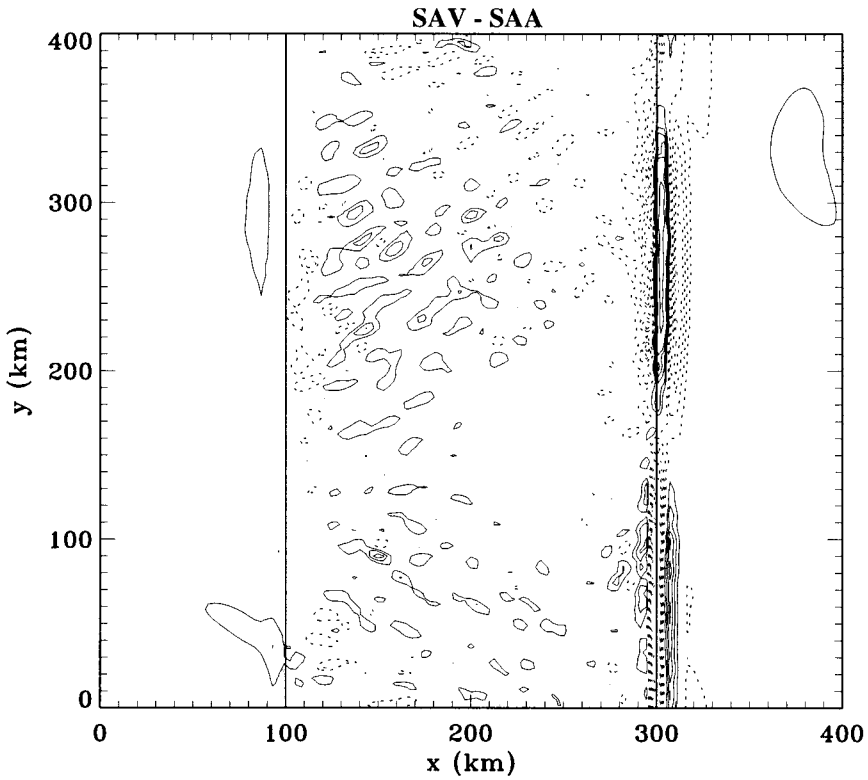

FIG. 13. Difference in low-level convergence below 440-m altitude at 1000 LST between simulations SAV and SAA. Solid contour lines indicate stronger convergence for SAV, and dotted lines indicate stronger convergence for SAA. The contour interval is 0.0003 s^{-1}.

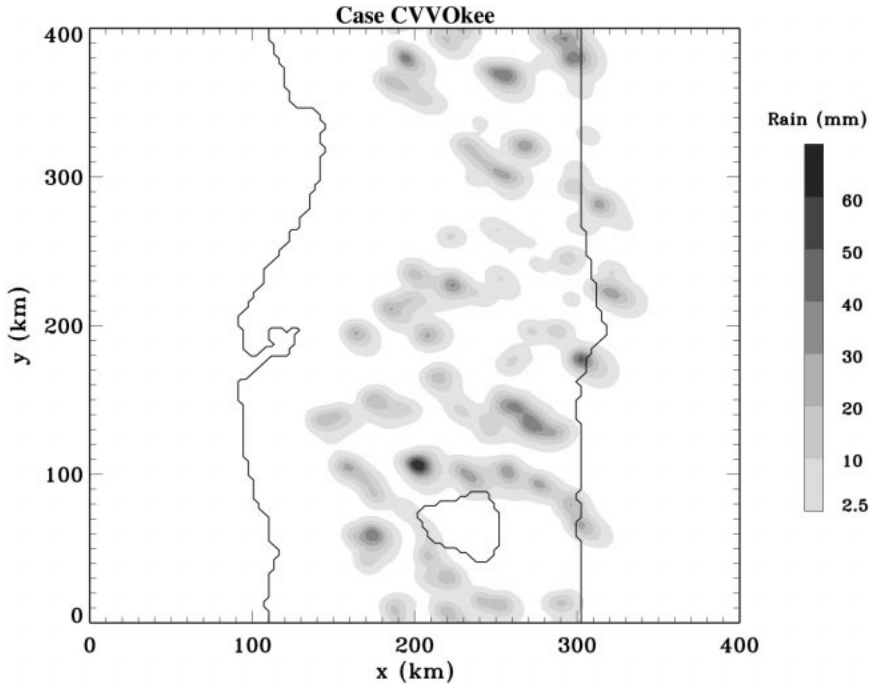

FIG. 14. Accumulated rainfall from 0600 to 2100 LST for simulation CVVOkee.

form precipitation. Last, synoptic-scale forcing may have played a role in squall line development over central Florida on 27 July 1991. The southernmost portion of a 700-hPa westerly trough extended into central Florida at 0700 LST. This trough produced weak midlevel divergence over the Florida peninsula, perhaps enhancing uplift and later squall line formation (Halverson et al. 1996).

Our simulations consider a single vegetation type: tall broadleaf trees with ground cover. In reality, the Florida peninsula experiences a wide range of land use, including swamps and marshes, cropland, deciduous forests, and evergreen forests. Although normally distributed statistical properties of land surface characteristics are utilized in our simulations (Table 2) to provide surface heterogeneity, they cannot account for the full range of land cover in Florida. This diversity in land use could have a major impact on cloud development and precipitation. For example, Pielke et al. (1999) show that land cover change in south Florida over the past 100 yr from natural vegetation to urban and agricultural use may account for reduced precipitation in recent years. In terms of our simulations, inclusion of wetlands would be likely to produce more precipitation because of increased soil moisture, whereas inclusion of urban areas would possibly reduce precipitation because of reduced evapotranspiration.

The sensitivity of our simulations to initial soil moisture and winds has implications for severe storm forecasting. Initial conditions with high spatial resolution are required for good forecasts. Dense sounding networks augmented by satellite wind estimates and regional-scale model output may be used for improved wind initial conditions (e.g., Velden et al. 1997). Microwave satellite estimates of soil moisture can provide wide spatial coverage at moderately high resolution (~30 km; Lakshmi et al. 1997). In addition, high-resolution estimates of precipitation from rain gauges, radar, and satellites (e.g., Tropical Rainfall Measuring Mission and Global Precipitation Mission) can be put into offline land surface models such as PLACE to provide high-resolution soil moisture initial conditions for fully coupled atmosphere–land surface models. This method offers the advantage of using consistent physics parameterizations for initial conditions and for model forecasts.

6. Summary

Idealized numerical simulations have been performed with a coupled atmosphere–land surface model (GCE–PLACE) to test the effects of soil moisture, coastline curvature, and land breezes on sea-breeze-initiated precipitation. The key results are summarized in Table 3 and below.

1) The distribution of initial soil moisture influences the timing and location of precipitation. The heaviest precipitation preferentially occurs over wet soil. Soil moisture acts as an atmospheric moisture source and increases the convectively available potential energy. Mesoscale circulations induced by soil moisture gradients do not produce heavy precipitation in our simulations.
2) Coastline curvature affects the timing and location of precipitation by inducing earlier low-level convergence near regions with convex curvature. The heaviest precipitation occurs near convex coastlines.
3) Early-morning land-breeze circulations cause earlier heavy precipitation by influencing the timing of strong low-level convergence.
4) Nonlinear interaction between coastline curvature and initial soil moisture produces extremely heavy precipitation near regions of wet soil. Simulations with coastline curvature or soil moisture variations alone do not account for this heavy rainfall. The combination of coastline curvature and early-morning land breezes causes a significant change in the location of heavy precipitation because of localized convergence along the east-coast sea-breeze front.
5) Lake Okeechobee affects the timing and location of heavy precipitation by producing strong lake-breeze circulations.

Acknowledgments. This paper greatly benefited from useful discussions with Jeffrey Halverson, Brad Ferrier, Peter Wetzel, Stephen Lang, and Daniel Johnson. We also thank three anonymous reviewers for their constructive comments. This work is supported by the NASA Headquarters (HQ) Physical Climate Program. We thank Dr. R. Kakar (HQ) for his support.

REFERENCES

Atkins, N. T., and R. M. Wakimoto, 1997: Influence of the synoptic-scale flow on sea breezes observed during CaPE. *Mon. Wea. Rev.,* **125,** 2112–2130.

Avissar, R., and Y.-Q. Liu, 1996: Three-dimensional numerical study of shallow convective clouds and precipitation induced by land surface forcing. *J. Geophys. Res.,* **101,** 7499–7518.

Beljaars, A. C. M., P. Viterbo, M. J. Miller, and A. K. Betts, 1996: The anomalous rainfall over the United States during July 1993: Sensitivity to land surface parameterization and soil moisture anomalies. *Mon. Wea. Rev.,* **124,** 362–383.

Blanchard, D. O., and R. E. Lopez, 1985: Spatial patterns of convection in south Florida. *Mon. Wea. Rev.,* **113,** 1282–1299.

Boybeyi, Z., and S. Raman, 1992: A three-dimensional numerical sensitivity study of convection over the Florida peninsula. *Bound.-Layer Meteor.,* **60,** 325–359.

Businger, J. A., J. C. Wyngaard, Y. Izumi, and E. F. Bradley, 1971: Flux-profile relationships in the atmospheric surface layer. *J. Atmos. Sci.,* **28,** 181–189.

Byers, H. R., and H. R. Rodebush, 1948: Causes of thunderstorms of the Florida peninsula. *J. Meteor.,* **5,** 275–280.

Chen, T. H., and Coauthors, 1997: Cabauw experimental results from the Project for Intercomparison of Land Surface Parameterization Schemes. *J. Climate,* **10,** 1194–1215.

Clark, C. A., and R. W. Arritt, 1995: Numerical simulations of the effect of soil moisture and vegetation cover on the development of deep convection. *J. Appl. Meteor.,* **34,** 2029–2045.

Crook, N. A., 1996: Sensitivity of moist convection forced by boundary layer processes to low-level thermodynamic fields. *Mon. Wea. Rev.*, **124,** 1767–1785.

Doran, J. C., and Coauthors, 1992: The Boardman regional flux experiment. *Bull. Amer. Meteor. Soc.,* **73,** 1785–1795.

Eltahir, E. A. B., 1998: A soil moisture–rainfall feedback mechanism. 1. Theory and observations. *Water Resour. Res.,* **34,** 765–776.

Fankhauser, J. C., N. A. Crook, J. Tuttle, L. J. Miller, and C. G. Wade, 1995: Initiation of deep convection along boundary layer convergence lines in a semitropical environment. *Mon. Wea. Rev.*, **123,** 291–313.

Ferrier, B. S., W.-K. Tao, and J. Simpson, 1995: A double-moment multiple-phase four-class bulk ice scheme. Part II: Simulations of convective storms in different large-scale environments and comparisons with other bulk parameterizations. *J. Atmos. Sci.*, **52,** 1001–1033.

Findell, K. L., and E. A. B. Eltahir, 1997: An analysis of the soil moisture–rainfall feedback, based on direct observations from Illinois. *Water Resour. Res.,* **33,** 725–735.

Halverson, J., M. Garstang, J. Scala, and W.-K. Tao, 1996: Water and energy budgets of a Florida mesoscale convective system: A combined observational and modeling study. *Mon. Wea. Rev.*, **124,** 1161–1180.

Kingsmill, D. E., 1995: Convection initiation associated with a seabreeze front, a gust front, and their collision. *Mon. Wea. Rev.*, **123,** 2913–2933.

Lakshmi, V., E. F. Wood, and B. J. Choudhury, 1997: Evaluation of Special Sensor Microwave/Imager satellite data for regional soil moisture estimation over the Red River basin. *J. Appl. Meteor.*, **36,** 1309–1328.

Lin, Y.-L., R. D. Rarley, and H. D. Orville, 1983: Bulk parameterization of the snow field in a cloud model. *J. Climate Appl. Meteor.,* **22,** 1065–1092.

Lynn, B. H., W.-K. Tao, and P. Wetzel, 1998: A study of landscape-generated deep moist convection. *Mon. Wea. Rev.,* **126,** 928–942.

McPherson, R. D., 1970: A numerical study of the effect of a coastal irregularity on the sea breeze. *J. Appl. Meteor.*, **9,** 767–777.

Meeson, B. W., F. E. Corprew, J. M. P. McManus, D. M. Meyers, J. W. Closs, K.-J. Sun, D. J. Sunday, and P. J. Sellers, 1995: *ISLSCP Initiative I: Global Data Sets for Land-Atmosphere Models, 1987–1988.* Vols. 1–5, NASA, CD-ROM.

Moncrieff, M., S. K. Krueger, D. Gregory, J. L. Redelsperger, and W. K. Tao, 1997: GEWEX Cloud System Study (GCSS) Working Group 4: Precipitating convective cloud systems. *Bull. Amer. Meteor. Soc.,* **78,** 831–845.

Nair, U. S., M. R. Hjelmfelt, and R. A. Pielke Sr., 1997: Numerical simulation of the 9–10 June 1972 Black Hills storm using CSU RAMS. *Mon. Wea. Rev.,* **125,** 1753–1766.

Nicholls, M. E., R. Pielke, and W. Cotton, 1991: A two-dimensional numerical investigation of the interaction between sea breezes and deep convection over the Florida pennisula. *Mon. Wea. Rev.*, **119,** 298–323.

Ookouchi, Y., M. Segal, R. C. Kessler, and R. A. Pielke, 1984: Evaluation of soil moisture effects on the generation and modification of mesoscale circulations. *Mon. Wea. Rev.,* **112,** 2281–2292.

Pielke, R. A., 1974: A three-dimensional numerical model of the sea breezes over south Florida. *Mon. Wea. Rev.,* **102,** 115–139.

Pielke, R. A. Sr., R. L. Walko, L. T. Steyaert, P. L. Vidale, G. E. Liston, W. A. Lyons, and T. N. Chase, 1999: The influence of anthropogenic landscape changes on weather in south Florida. *Mon. Wea. Rev.,* **127,** 1663–1673.

Rabin, R., S. Stadler, P. Wetzel, D. Stensrud, and M. Gregory, 1990: Observed effects of landscape variability on convective clouds. *Bull. Amer. Meteor. Soc.,* **71,** 272–280.

Rao, P. A., H. E. Fuelberg, and K. K. Droegemeier, 1999: High-resolution modeling of the Cape Canaveral area land–water circulations and associated features. *Mon. Wea. Rev.,* **127,** 1808–1821.

Rotunno, R., J. B. Klemp, and M. L. Weisman, 1988: A theory for strong, long-lived squall lines. *J. Atmos. Sci.,* **45,** 463–485.

Rutledge, S. A., and P. V. Hobbs, 1984: The mesoscale and microscale structure and organization of clouds and precipitation in midlatitude cyclones. Part XII: A diagnostic modeling study of precipitation development in narrow cold frontal rainbands. *J. Atmos. Sci.,* **41,** 2949–2972.

Segal, M., and R. W. Arritt, 1992: Nonclassical mesoscale circulations caused by surface sensible heat-flux gradients. *Bull. Amer. Meteor. Soc.*, **73,** 1593–1604.

——, ——, C. Clark, R. Rabin, and J. Brown, 1995: Scaling evaluation of the effect of surface characteristics on potential for deep convection over uniform terrain. *Mon. Wea. Rev.,* **123,** 383–400.

Simpson, J., and W.-K. Tao, 1993: Goddard Cumulus Ensemble Model. Part II: Applications for studying cloud precipitating processes and for NASA TRMM. *Terr. Atmos. Oceanic Sci.,* **4,** 73–116.

——, N. E. Westcott, R. J. Clerman, and R. A. Pielke, 1980: On cumulus mergers. *Arch. Meteor. Geophys. Bioklimatol.,* **29,** 1–40.

Tao, W.-K., and J. Simpson, 1989: A further study of cumulus interactions and mergers: Three-dimensional simulations with trajectory analyses. *J. Atmos. Sci.,* **46,** 2974–3004.

——, and ——, 1993: Goddard Cumulus Ensemble Model. Part I: Model description. *Terr. Atmos. Oceanic Sci.,* **4,** 35–72.

Taylor, C. M., F. Said, and T. Lebel, 1997: Interactions between the land surface and mesoscale rainfall variability during HAPEX-Sahel. *Mon. Wea. Rev.,* **125,** 2211–2227.

Ulanski, S. L., and M. Garstang, 1978: The role of surface divergence and vorticity in the life cycle of convective rainfall. Part I: Observation and analysis. *J. Atmos. Sci.,* **35,** 1047–1062.

Velden, C. S., C. M. Hayden, S. J. Nieman, W. P. Menzel, S. Wanzong, and J. S. Goerss, 1997: Upper-tropospheric winds derived from geostationary satellite water vapor observations. *Bull. Amer. Meteor. Soc.*, **78,** 173–195.

Weisman, M. L., W. C. Skamarock, and J. B. Klemp, 1997: The resolution dependence of explicitly modeled convective systems. *Mon. Wea. Rev.,* **125,** 527–548.

Wetzel, P., and A. Boone, 1995: A Parameterization for Land–Atmosphere–Cloud Exchange (PLACE): Documentation and testing of a detailed process model of the partly cloudy boundary layer over heterogeneous land. *J. Climate,* **8,** 1810–1837.

Wilson, J. W., and D. L. Megenhardt, 1997: Thunderstorm initiation, organization, and lifetime associated with Florida boundary layer convergence lines. *Mon. Wea. Rev.,* **125,** 1507–1525.

Woodruff, S. D., S. J. Lubker, K. Wolter, S. J. Worley, and J. D. Elms, 1993: Comprehensive Ocean–Atmosphere Data Set (COADS) Release 1a: 1980–92. *Earth Syst. Monit.,* **4,** 1–8.

Xu, L., S. Raman, R. V. Madala, and R. Hodur, 1996: A non-hydrostatic modeling study of surface moisture effects on mesoscale convection induced by sea breeze circulation. *Meteor. Atmos. Phy.,* **58,** 103–122.

Yan, H., and R. A. Anthes, 1988: The effect of variations in surface moisture on mesoscale circulations. *Mon. Wea. Rev.,* **116,** 192–208.

Zilitinkevich, S. S., 1975: Comments on ''A model for the dynamics of the inversion above a convective boundary layer.'' *J. Atmos. Sci.,* **32,** 991–992.